Journal of Theoretical and Applied Physics (2020) 14:295–305
https://doi.org/10.1007/s40094-020-00383-4

RESEARCH

Temperature dependence of EXAFS spectra of BCC crystals analyzed based on classical anharmonic correlated Einstein model

Tong Sy Tien[1]

Received: 24 December 2019 / Accepted: 18 June 2020 / Published online: 27 July 2020

Abstract
In this work, the temperature dependence of extended X-ray absorption fine structure (EXAFS) of the body-centered cubic crystals was investigated based on the anharmonic correlated Einstein model using the classical statistical theory. The oscillation of the anharmonic EXAFS spectra presented in terms of the cumulant expansion up to the fourth order. Here, the thermodynamic parameters of a system are derived from an anharmonic effective potential that has taken into account the influence of all nearest neighbors of absorbing and backscattering atoms. Analytical expressions of the first four EXAFS cumulants are obtained in simple forms of temperature or parallel mean-square relative displacement. The numerical results for crystalline molybdenum in the temperature range from 0 to 900 K are found to be in good agreement with those obtained using the other theoretical methods and experiments at various temperatures. The analytical results for the contributions of the cumulants to the amplitude reduction and phase shift of the EXAFS oscillation discover the role and meaning of high-order cumulants in analyzing the temperature dependence of the EXAFS spectra.

Keywords EXAFS spectra · BCC crystals · Anharmonic correlated Einstein model · Classical statistical theory

Introduction

The extended X-ray absorption fine structure (EXAFS) has been developed into a powerful technique and widely used for determining many structural parameters and dynamic properties of disordered materials. They are related to the local environment surrounding a specific atomic species such as the number, type, and position of the central-atom neighbors, and the relative vibrational amplitudes and force constants of the neighbor atoms [1–5]. The EXAFS oscillation for a single coordination shell has the form $\chi(k) = A(k)\sin\Phi(k)$, where $A(k)$ and $\Phi(k)$ are the EXAFS amplitude and phase, respectively [6–9]. There is the fact that the atoms are not stationary, the position and interatomic distance of atoms are changed due to thermal vibrations at any temperature [6, 7]. The sensitivity of the EXAFS spectra to thermal vibrations was detected by Beni and Platzman (1976) [2] and discussed detail by Eisenberger and Brown (1979) [3]. These thermal vibrations cause thermal disorder and anharmonic effects on lattice vibrations and will smear out the EXAFS spectra [3, 6].

In a solid, the exhibiting local dynamic disorder of the atomic positions around a central atom has to be described in terms of the radial distribution function (RDF) [3–6], and the moments of RDF (or cumulants) are determined more stable and interpreted more naturally by Kubo [10]. The use of the cumulants in investigating the local disorder of the EXAFS spectra was introduced by Rehr [11] who showed that the Debye–Waller factor (DWF) in the EXAFS spectra has a natural cumulant expansion in powers of the photoelectron wavenumber [12]. The DWF was described detail in the cumulant expansion approach (*ratio* method) by Bunker [7] and exploited by Tranquada and Ingalls [13], which can be viewed as a result of averaging the single-scattering EXAFS formula over many near-neighbor pairs with a given RDF by Crozier et al. [14]. An account of the DWF with the local disorder is especially crucial for achieving the correct EXAFS amplitudes, and an account of the anharmonicity is essential for a proper understanding of the EXAFS phase [7, 11]. Further, the importance of including higher-order cumulants (the third and fourth cumulants) in the anharmonic EXAFS analysis has been recognized in many works [15–19]. In these works, the *ratio* method is

✉ Tong Sy Tien
tongsytien@duytan.edu.vn

[1] Institute of Research and Development, Duy Tan University, Da Nang 550000, Vietnam

particularly appealing because it summarizes the relevant structural and dynamic information in a few parameters that are easily obtained from the experimental EXAFS spectra [8, 9, 20, 21].

Unfortunately, the dynamical matrix or even the local spring constants are not known in most cases of interest, and hence in practice, one must often rely on simpler, phenomenological approximations [11]. Two such methods are the correlated Debye (CD) and correlated Einstein (CE) models that were modified by Beni & Platzman (1976) [2] and Sevillano et al. (1979) [22] from the conventional Debye and Einstein models, respectively. These models are based on the expansion of the anharmonic EXAFS oscillation as a series of cumulants and have achieved effective certain [14]. However, the applicability of them for tridimensional systems was discussed by Miyanaga and Fujikawa [23–25] who showed that simple approximation of these models gives rather poor results not only for the third- and fourth-order cumulants but also for the anharmonic correction of the second-order cumulant.

Additionally, many theoretical approaches have been used to calculate and evaluate the contribution of thermal vibrations to the anharmonic EXAFS spectra. The quantum approaches [24–33] took into account the quantum effects at low temperatures and the anharmonic effects at high temperatures. However, they still have some limitations as the results of the EXAFS cumulants not being expressed in explicit forms. These limitations lead to complexity in determining thermodynamic parameters from the analysis of the anharmonic EXAFS spectra. It is because this work needs many computational steps with various parameters. The classical approach using a classical approximation based on the force constants of an effective potential was proposed by Stern et al. [34], in which the parameters of the interatomic potential of the system are unknown. This method can calculate the temperature dependence of the EXAFS cumulants up to the fourth order and obtain results in simple forms. It works well at high temperatures, and it was used effectively for analyzing anharmonic EXAFS spectra of some crystals [21, 35–37].

For many-atom systems, the EXAFS cumulants are often connected to the force constants of a one-dimensional model of the effective pair potential by the analytical expressions similar to those for two-atom systems [12, 25]. However, the connection between the EXAFS cumulants and the thermodynamic parameters of many-atom systems remains a matter of great interest [11, 25], especially regarding the meaning of effective potential [38, 39]. The sensitivity of the EXAFS cumulants with the nature of the bonding potential of atoms was suggested by Rehr et al. [40]. Then, the anharmonic effective (AE) potential is derived from the first shell near-neighbor contribution approach and the anharmonic effects. It was instituted by Hung and Rehr [12] who proposed an anharmonic correlated Einstein (ACE) model based on the AE potential using the first-order thermodynamic perturbation theory [17].

Recently, the anharmonic correlated Debye (ACD) model based on the correlated Debye model [2] and many-body perturbation approach [41] using the AE potential proposed by Hung et al. [33]. It was successfully applied to investigate the anharmonic EXAFS spectra for body-centered cubic (BCC) crystals [42] and face-centered cubic (FCC) crystals [43–45]. Still, the analytical expressions of the EXAFS cumulants are not in explicit forms, so the analysis of the anharmonic EXAFS spectra requires much computational effort. The ACE model [12] using the quantum statistical theory (henceforth cited as the QACE model), it was successfully applied to calculate and evaluate the EXAFS spectra for various crystal structures [46–51], but it only extends the EXAFS cumulants up to the third order and has not yet analyzed the anharmonic EXAFS spectra. The ACE model [12] using the classical statistical theory [34] (henceforth cited as the CACE model), it was efficiently used to investigate and evaluate the anharmonic EXAFS spectra for hexagonal close-packed (HCP) crystals by Hung et al. [38] and diamond (DIA) crystals by Tien et al. [39]. Still, it has not been used to investigate for BCC crystals and considered the contribution of the cumulants to the anharmonic EXAFS amplitude and phase. Meanwhile, the experimental EXAFS spectra of BCC crystals were analyzed using the cumulant expansion approach up to the fourth order [36]. Therefore, the development of a CACE model to efficiently calculate and analyze the temperature dependence of the EXAFS spectra of BCC crystals, which will be a necessary addition to the EXAFS technique.

The purpose of this work is to develop a more suitable calculation model based on the CACE model for the anharmonic EXAFS data analysis of the first coordination shell of BCC crystals. In this work, the AE potential is expanded up to the fourth order instead of lower orders, and the Morse potential characterizes the interaction between a pair of atoms. The temperature dependence of the first four cumulants and the EXAFS amplitude and phase is calculated and described in simple forms. Our numerical results for crystalline molybdenum (Mo) are found to be in good agreement with those obtained using the QACE model [51], the ACD model [42] and experiments [36] at various temperatures. From evaluating the contribution of the cumulants to the amplitude reduction and phase shift of the EXAFS oscillation, we discovered the role and meaning of the cumulants in analyzing the anharmonic EXAFS spectra.

This article is organized as follows. The theoretical model and basic formulae of the EXAFS oscillation are introduced in second section. Third section calculates the anharmonic effective potential and the first four cumulants of the EXAFS spectra of BCC crystals based on the CACE model. The

numerical results for Mo compared with those other theoretical methods and experiments are discussed in fourth section. Final section gives the main conclusions about this work.

Basic formulae of the anharmonic EXAFS oscillation

For the distribution of identical atoms and including non-Gaussian disorder, the *K*-edge EXAFS oscillation of polycrystalline materials is described within the framework of single-scattering and plane-wave approximations by [7, 13, 14]

$$\chi(k) = \frac{NS_0^2(k)}{k}F(k)\mathrm{Im}\left\{\left\langle \frac{e^{-2r/\lambda(k)}}{r^2}\mathrm{e}^{2ikr}\right\rangle e^{i\delta(k)}\right\}, \tag{1}$$

where k is the photoelectron wave number, $\lambda(k)$ is the electron mean free path, N is the coordination number, $F(k)$ is the atomic backscattering amplitude, $\delta(k)$ is the net phase shift, the angular brackets $\langle\ \rangle$ are the thermal average, $S_0^2(k)$ is an amplitude reduction factor due to the many-body effects, and r depends on the temperature T and is the instantaneous distance between the absorber atom and one neighboring atom.

The normalized *K*-edge EXAFS oscillation $k^2\chi(k)$ of Mo is shown in Fig. 1. It can be seen the anharmonic effects caused by thermal vibrations that significantly influence the EXAFS oscillation. The influence of these effects increases the amplitude reduction and phase shift of the EXAFS oscillation. At the higher temperature, the stronger the influence on the anharmonic EXAFS amplitude and phase is [11, 13, 14].

Using the cumulant expansion approach in powers of k [7, 11, 14] to expand the asymmetric terms in the brackets of Eq. (1) in a Taylor series about R and rewrites the thermal

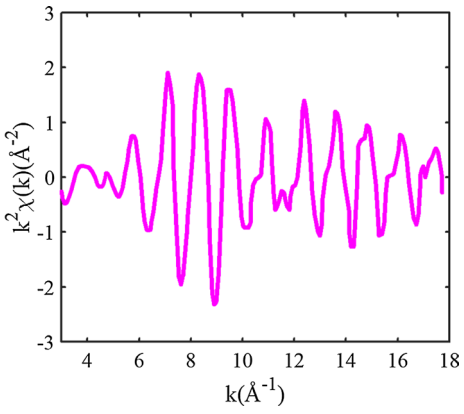

Fig. 1 The normalized *K*-edge EXAFS oscillation $k^2\chi(k)$ of Mo measured at 573 K [36]

average in terms of cumulants [8, 52], if the small-terms yield from the mean free path (which implies a complex k) are neglected and approximated expansion to the fourth cumulant, the result can be obtained as

$$\left\langle \frac{e^{-2r/\lambda}}{r^2}\mathrm{e}^{2ikr}\right\rangle \approx \frac{e^{-2R/\lambda}}{R^2}\exp\left\{2ikr_0 + 2k\sigma^{(1)} - 2k^2\sigma^2 - 4ik\sigma^2\left(\frac{1}{R}+\frac{1}{\lambda}\right) - \frac{4i}{3}k^3\sigma^{(3)} + \frac{2}{3}k^4\sigma^{(4)}\right\}, \tag{2}$$

where r_0 is the equilibrium distance between the absorbing and backscattering atoms, and the coefficients $\sigma^{(n)}$ depend on the temperature T and are the cumulants.

The analysis of the temperature dependence of the EXAFS spectra involves the EXAFS cumulants, in which the even-order cumulants contribute primarily to the EXAFS amplitude, and the odd-order cumulants contribute mainly to the EXAFS phase. A usual EXAFS analysis uses the first four cumulants that are given by [8, 11, 14, 53]

$$\sigma^{(1)} = \langle r\rangle - r_0, \tag{3}$$

$$\sigma^{(2)} \equiv \sigma^2 = \left\langle (r-R)^2\right\rangle, \tag{4}$$

$$\sigma^{(3)} = \left\langle (r-R)^3\right\rangle, \tag{5}$$

$$\sigma^{(4)} = \left\langle (r-R)^4\right\rangle - 3\left(\sigma^2\right)^2, \tag{6}$$

where the second cumulant σ^2 is the parallel mean-square relative displacement (MSRD) of the effective path length associated with a given multiple-scattering (MS) path, and the average distance between central and backscattering atom is $R = \langle r\rangle = \frac{1}{N}\int_0^\infty \rho(T,r)r\mathrm{d}r$ with $\rho(T,r)$ is true RDF [8].

Replacing Eq. (2) with Eq. (1), we obtain the formalism of the *K*-edge EXAFS function, including the anharmonic effects as

$$\chi(k) \cong \frac{NS_0^2(k)e^{-2R/\lambda}}{kR^2}F(k)\exp\left\{-2k^2\sigma^2 + \frac{2k^4}{3}\sigma^{(4)}\right\} \sin\left\{2kr_0 + 2k\sigma^{(1)} - 4k\sigma^2\left(\frac{1}{R}+\frac{1}{\lambda}\right) - \frac{4k^3}{3}\sigma^{(3)} + \delta(k)\right\}. \tag{7}$$

Then, the temperature T and wavenumber k dependence of the amplitude $A(k,T)$ and phase $\Phi(k,T)$ is deduced from Eq. (7) as follows:

$$A(k,T) = \frac{NS_0^2(k)e^{-2R(T)/\lambda(k)}}{kR^2(T)}F(k)\times\exp\left\{-2k^2\sigma^2(T) + \frac{2k^4}{3}\sigma^{(4)}(T)\right\}, \tag{8}$$

$$\Phi(k,T) = 2kr_0 + 2k\sigma^{(1)}(T) - 4k\sigma^2(T)\left\{\frac{1}{R(T)} + \frac{1}{\lambda(k)}\right\} - \frac{4k^3}{3}\sigma^{(3)}(T) + \delta(k). \quad (9)$$

Thus, the anharmonic EXAFS spectra can be analyzed based on the temperature dependence of the first four cumulants via Eqs. (8) and (9). It indicates that the lack of precise EXAFS cumulants is one of the most significant limitations to accurate structural determinations (for example, the coordination number and interatomic distances) from the experimental EXAFS data [31, 32]. The structural parameters of materials can be obtained by analyzing the experimental EXAFS data with well-established procedures [26, 53]. As can be seen from Eqs. (8) and (9), the anharmonicity of the potential yields additional terms in the anharmonic EXAFS amplitude and phase [3, 5, 11]. If ignoring these terms, it can lead to non-negligible errors in the structural parameters [11–14].

Model of calculating the anharmonic EXAFS cumulants

Anharmonic effective potential in the ACE model

In order to determine the thermodynamic parameters of a system, it is necessary to specify its AE potential and force constants [12, 38, 39]. One considers a monatomic system with an AE potential (ignored the constant contribution) is extended up to the fourth order:

$$V_{\text{eff}}(x) = \frac{1}{2}k_0x^2 - k_3x^3 + k_4x^4, \quad (10)$$

where $x = r - r_0$ is the deviation of the interatomic distance from the potential minimum position, k_0 is the effective force constant, and k_3 and k_4 are local force constants giving the asymmetry of potential due to the inclusion of anharmonicity.

The Morse potential is assumed to describe the interatomic interaction model for the potential energy of a diatomic molecule [54]. It is given in terms of the function by

$$V(x) = D\left(e^{-2\alpha x} - 2e^{-\alpha x}\right), \quad (11)$$

where x is the same previously defined value, α describes the width of the potential, and D is the dissociation energy.

Applying the Morse potential to calculate the interaction energy between each pair of atoms in cubic metals, which was proposed by Girifalco and Weizer [55]. In the present procedure, we expand the Morse potential to the fourth order:

$$V(x) \cong -D + D\alpha^2x^2 - D\alpha^3x^3 + \frac{7}{12}D\alpha^4x^4. \quad (12)$$

In the relative vibrations of absorbing (A) and backscattering (B) atoms, including the effect of correlation and taking into account only the nearest-neighbor interactions, the AE potential [12] is given by

$$V_{\text{eff}} = V(x) + \sum_{i=A,B}\sum_{j\neq A,B} V\left(\frac{\mu}{M_i}x\hat{R}_{AB}\hat{R}_{ij}\right), \quad (13)$$

where M_i is a mass of the i th atom, $\mu = M_AM_B/(M_A + M_B)$ is the reduced mass of the absorber and backscatterer with masses M_A and M_B, respectively, $\hat{R}$ is a unit vector, the sum i is the over absorbers ($i = A$) and backscatterers ($i = B$), and the sum j is over the nearest neighbors.

As can be seen on the right side of Eq. (13), the first term concerns only the pair interaction potential of the absorbing and backscattering atoms. And the second describes the contribution of their nearest-neighbor atoms to the pair interaction potential and depends on the crystal structure.

The model of the BCC crystal structures of Mo is illustrated in Fig. 2. It can be seen that each atom is bonded with other surrounding eight atoms and are arranged in a variation. For the monatomic crystals, all atoms are the same, so their mass is equal and has a value of $M_i = m$. Applying Eq. (13) to these crystals, the AE potential is written as

$$V_{\text{eff}}(x) = V(x) + V(0) + 2V\left(-\frac{1}{2}x\right) + 6V\left(-\frac{1}{6}x\right) + 6V\left(\frac{1}{6}x\right). \quad (14)$$

Using the Morse potential in Eq. (12) to calculate the AE potential according to Eq. (14) and ignoring the overall constant, we obtain the result as

$$V_{\text{eff}}(x) = \frac{11}{6}D\alpha^2x^2 - \frac{3}{4}D\alpha^3x^3 + \frac{1715}{2592}\alpha^4x^4. \quad (15)$$

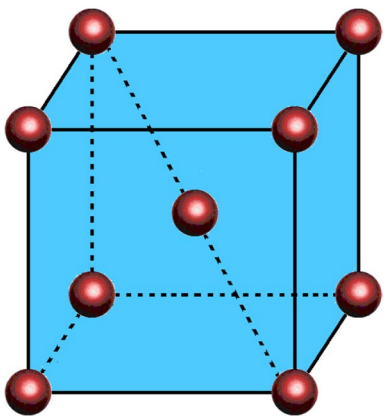

Fig. 2 Model of the BCC crystals

Comparing Eq. (10) with Eq. (15), we deduce the local force constants k_0, k_3, and k_4 as follows:

$$k_0 = \frac{11}{3}D\alpha^2, \quad k_3 = \frac{3}{4}D\alpha^3, \quad k_4 = \frac{1715}{2592}D\alpha^4. \tag{16}$$

The thermal vibrations of atoms are characterized by the correlated Einstein frequency ω_E and temperature θ_E that are calculated from the effective force constant k_0 in the following forms:

$$\omega_E = \sqrt{\frac{k_0}{\mu}} = \sqrt{\frac{22D\alpha^2}{3m}}, \quad \theta_E = \frac{\hbar\omega_E}{k_B}, \tag{17}$$

where k_B is the Boltzmann constant, $\hbar$ is the reduced Planck constant.

Consequently, the correlated Einstein frequency ω_E and temperature θ_E, and local the force constants k_0, k_3, and k_4 are expressed in terms of the Morse potential parameters.

Temperature dependence of EXAFS cumulants within a classical statistical theory

The EXAFS cumulants are explicitly related to low-order moments of effective RDF [8, 23]. Hence we can express the first four cumulants from Eqs. (3) to (6) in terms of moments $\langle x^n\rangle$ ($k=1$, 2, 3, and 4) as follows:

$$\sigma^{(1)} = \langle x\rangle, \tag{18}$$

$$\sigma^2 = \left\langle (x-\langle x\rangle)^2\right\rangle = \left\langle x^2\right\rangle - \langle x\rangle^2, \tag{19}$$

$$\sigma^{(3)} = \left\langle (x-\langle x\rangle)^3\right\rangle = \left\langle x^3\right\rangle - 3\left\langle x^2\right\rangle\langle x\rangle + 2\langle x\rangle^3, \tag{20}$$

$$\sigma^{(4)} = \left\langle (x-\langle x\rangle)^4\right\rangle - 3\left[\left\langle (x-\langle x\rangle)^2\right\rangle\right]^2 = \left\langle x^4\right\rangle + 12\left\langle x^2\right\rangle\langle x\rangle^2 - 3\left\langle x^2\right\rangle^2 - 4\left\langle x^3\right\rangle\langle x\rangle - 6\langle x\rangle^4. \tag{21}$$

Using the effective anharmonic potential in Eq. (10) within the classical statistical theory and assuming that anharmonicity can be treated as a small perturbation, we determine the moments about the mean $\langle x^n\rangle$ by evaluating the thermal average in the third-order approximation [34]:

$$\langle x^n\rangle = \frac{\int_{-\infty}^{\infty} x^n \exp\left[-\frac{V_{\text{eff}}(x)}{k_BT}\right]dx}{\int_{-\infty}^{\infty}\exp\left[-\frac{V_{\text{eff}}(x)}{k_BT}\right]dx} \approx \frac{\int_{-\infty}^{\infty} x^n \exp\left[\frac{-k_0x^2}{2k_BT}\right]\left[\sum_{n=0}^{3}\frac{1}{n!}\left(\frac{k_3x^3-k_4x^4}{k_BT}\right)^n\right]dx}{\left(\frac{2\pi k_BT}{k_0}\right)^{1/2}\left[1+\frac{3(k_BT)}{k_0^2}\left(\frac{5k_3^2}{2k_0}-k_4\right)\right]}. \tag{22}$$

To obtain the temperature dependence of the first four EXAFS cumulants from Eqs. (18) to (21), we use Eq. (16) to calculate the moments $\langle x^n\rangle$ according to Eq. (22), the obtained expressions of the cumulants in the lowest orders are

$$\sigma^{(1)} \simeq \frac{81k_BT}{484D\alpha}\left(1-\frac{203425k_BT}{191664D}\right), \tag{23}$$

$$\sigma^{(2)} \simeq \frac{3k_BT}{11D\alpha^2}\left(1-\frac{5743k_BT}{31944D}\right), \tag{24}$$

$$\sigma^{(3)} \simeq \frac{243(k_BT)^2}{2662D^2\alpha^3}\left(1-\frac{79567k_BT}{31944D}\right), \tag{25}$$

$$\sigma^{(4)} = \left\langle (x-\langle x\rangle)^4\right\rangle - 3\left(\sigma^2\right)^2 \simeq \frac{1227\,(k_BT)^3}{322102\,D^3\alpha^4}\left(1+\frac{3975025253\,k_BT}{69680512\,D}\right). \tag{26}$$

The truncation of the series in Eq. (22) serves as a convergence cutoff, while including enough terms to obtain the second lowest-order expressions for the moments accurately. Because $k_BT/D << 1$, the respective expressions obtained from Eqs. (23)–(26) in the lowest order as follows:

$$\sigma^{(1)} \approx \frac{81k_BT}{484D\alpha} = \frac{27\alpha}{44}\sigma^2, \tag{27}$$

$$\sigma^{(2)} \approx \frac{3k_BT}{11D\alpha^2} \equiv \sigma^2, \tag{28}$$

$$\sigma^{(3)} \approx \frac{243(k_BT)^2}{2662D^2\alpha^3} = \frac{27\alpha}{22}\left(\sigma^2\right)^2, \tag{29}$$

$$\sigma^{(4)} \approx \frac{1227\,(k_BT)^3}{322102\,D^3\alpha^4} = \frac{409\alpha^2}{2178}\left(\sigma^2\right)^3. \tag{30}$$

Thus, the temperature dependence of the first four EXAFS cumulants $\sigma^{(1)}$ and σ^2, $\sigma^{(3)}$, and $\sigma^{(4)}$ is proportional to T, T^2, and T^3, respectively, as can be seen from Eqs. (27) to (30). It also shows that the EXAFS cumulants are expressed in simple forms of parallel MSRD. These calculated results by the CACE model are similar to those

obtained using the QACE [51] and ACD [33, 42] models at high temperatures.

Assuming quantities $F(k)$, $\delta(k)$, $S_0^2(k)$, and $\lambda(k)$ in Eq. (7) to be the same at temperatures T_1 and T_2 [8, 21, 56], we deduce the logarithm of amplitude ratio $M(k,T_1,T_2)=\ln\left[A(k,T_2)/A(k,T_1)\right]$ and the phase difference $\Delta\Phi(k,T_1,T_2)=\Phi(k,T_2)-\Phi(k,T_1)$ between temperatures T_2 and T_1 from Eqs. (8) and (9) in the following forms:

$$M(k,T_1,T_2)\approx -2k^2\{\sigma^2(T_2)-\sigma^2(T_1)\}+\frac{2k^4}{3}\{\sigma^{(4)}(T_2)-\sigma^{(4)}(T_1)\}, \tag{31}$$

$$\Delta\Phi(k,T_1,T_2)\approx 2k\{\sigma^{(1)}(T_2)-\sigma^{(1)}(T_1)\}-4k\left\{\frac{1}{r_0}+\frac{1}{\lambda}\right\}\{\sigma^2(T_2)-\sigma^2(T_1)\}-\frac{4k^3}{3}\{\sigma^{(3)}(T_2)-\sigma^{(3)}(T_1)\}. \tag{32}$$

where the term $-2\{[R(T_2)-R(T_1)]/\lambda(k)+\ln[R(T_2)/R(T_1)]\}$ was neglected in Eq. (8) because it is insignificant compared to other terms in the equation, and the calculation of Eq. (9) used approximation $1/R(T)\ll 1/r_0$ with assuming $\sigma^{(1)}\ll r_0$ and $R(T)=r_0+\sigma^{(1)}$ are derived from Eq. (3).

As can be seen from Eqs. (27)–(30), the EXAFS cumulants at 0 K are all zero, so if we take $T_1=0K$ and reset $T_2=T$, the Eqs. (31) and (32) are rewritten as

$$M(k,T)=-2k^2\sigma^2(T)+\frac{2k^4}{3}\sigma^{(4)}(T), \tag{33}$$

$$\Delta\Phi(k,T)=2k\sigma^{(1)}(T)-4k\left\{\frac{1}{r_0}+\frac{1}{\lambda}\right\}\sigma^2(T)-\frac{4k^3}{3}\sigma^{(3)}(T). \tag{34}$$

Replacing the EXAFS cumulants in Eqs. (33) and (34) with the expressions determined by Eqs. (27)–(30), we obtain the following results:

$$M(k,T)=-\frac{6k_B}{11D\alpha^2}k^2T+\frac{409k_B^3}{161051\,D^3\alpha^4}T^3k^4, \tag{35}$$

$$\Delta\Phi(k,T)=\frac{81k_B}{242D\alpha}kT-\left(\frac{1}{r_0}+\frac{1}{\lambda}\right)\frac{12k_B}{11D\alpha^2}kT-\frac{162k_B^2}{1331D^2\alpha^3}k^3T^2. \tag{36}$$

Thus, the logarithm of amplitude ratio and the phase difference of the EXAFS oscillation are expressed in simple forms of temperature via the analytical expressions of the cumulants, as seen in Eqs. (35) and (36). These obtained results show that the cumulants are very useful for the quantitative treatment of the anharmonic EXAFS spectra.

Numerical results and discussions

In order to discuss the advancement of the present CACE model in this work for calculating and analyzing the temperature dependence of the EXAFS spectra, we apply the formulae in "Basic formulae of the anharmonic EXAFS oscillation" section and the analytical expressions in "Model of calculating the anharmonic EXAFS cumulants" section to numerical calculations for Mo. Firstly, we calculate the local force constants, the correlated Einstein frequency and temperature, and the position dependence of the Morse potential and the AE potential. Our results are compared with those obtained using the QACE model [51] and experiment [36]. Then, we calculate the temperature dependence of the first four EXAFS cumulants in the range from 0 to 900 K. Our results are compared with those obtained using the QACE [51] and ACD [42] models. Our results are also compared with the experimental values at seven different temperatures between 293 and 573 K. They were measured in transmission using the EXAFS spectrometer by Pirog et al. [36] at the Synchrotron Radiation Siberian Center, Russia. Lastly, we analyze the logarithm of amplitude ratio and the phase difference of the anharmonic EXAFS oscillation between temperatures 573 K and 0 K in the wavenumber range from 0 to 20 Å^{-1}. From the obtained results, we evaluate the

Table 1 The thermodynamic parameters k_0, k_3, k_4, ω_E, and θ_E of Mo obtained using the CACE model, the QACE model [51], and experiment [36]

Method	k_0 (eV Å^{-2})	k_3 (eV Å^{-3})	k_4 (eV Å^{-4})	ω_E ($\times 10^{13}$ Hz)	θ_E (K)
CACE model[a]	6.7	2.1	2.7	3.7	279.5
QACE model[b]	6.7	2.1		3.7	279.5
Experiment[c]	7.5	3.0	2.2	3.9	297.7

[a]This work

[b]Reference [51]

[c]Reference [36]

development and effectiveness of the CACE model for analyzing the temperature dependence of the EXAFS spectra.

The thermodynamic parameters k_0, k_3, k_4, ω_E, and θ_E for Mo are calculated by Eqs. (16) and (17) and given in Table 1, where the Morse potential parameters $D = 0.8032$ eV and $\alpha = 1.5079$ Å^{-1} derived from the experimental values of energy of vaporization [55]. Our results are compared with those obtained using the QACE model [51] and experiment [36]. The correlated Einstein frequency ω_E and temperature θ_E in Ref. [36] are deduced from the effective force constant k_0. As can be seen in Table 1, the values of thermodynamic parameters are no significant difference, especially for the correlated Einstein frequency ω_E, and temperature θ_E.

Figure 3a shows the position dependence of the Morse potential $V(x)$ of Mo. It can be seen that our calculated result using Eq. (12) agrees well with the results obtained using Eq. (11) with the experimental values of the Morse potential parameters [36] $D = 0.75$ eV and $\alpha = 1.44$ Å^{-1}, especially in the vicinity of the equilibrium bond lengths. In this comparison, our result also agrees more than the calculated result using the QACE model [51], as seen in Fig. 3a, which indicates that an approximate expansion of the Morse potential up to the fourth order is necessary. Figure 3b shows the position dependence of the AE potential $V_{\text{eff}}(x)$ of Mo. It can be seen that in comparison with the obtained result using Eq. (10) with the experimental values of the local force constants [36], our calculated results using Eq. (15) are in better agreement than the obtained result using the QACE model [51] that only takes into account the first two terms in Eq. (10). Additionally, as can be seen from Ref. [42], the ACD model also uses the Morse potential and AE potential that is derived from the same calculation model and parameter values as in the CACE model, so our results are similar to those obtained using the ACD model.

Thus, these comparison results show that the high-order terms cause the asymmetry of the AE potential, in which the fourth-order term contributes significantly to the anharmonicity composition.

Figure 4 shows the temperature dependence of the (a) first cumulant $\sigma^{(1)}(T)$ and (b) second cumulant $\sigma^2(T)$ of Mo calculated by Eqs. (27) and (28), respectively. At temperatures above $\theta_E \approx 279.5$ K, our calculated results using the CACE model indicate good agreement with those obtained using the QACE [51] model, the ACD [42] model, and experiment [36], as seen in Fig. 4. Here, the experimental values of Ref. [36] for the first cumulant

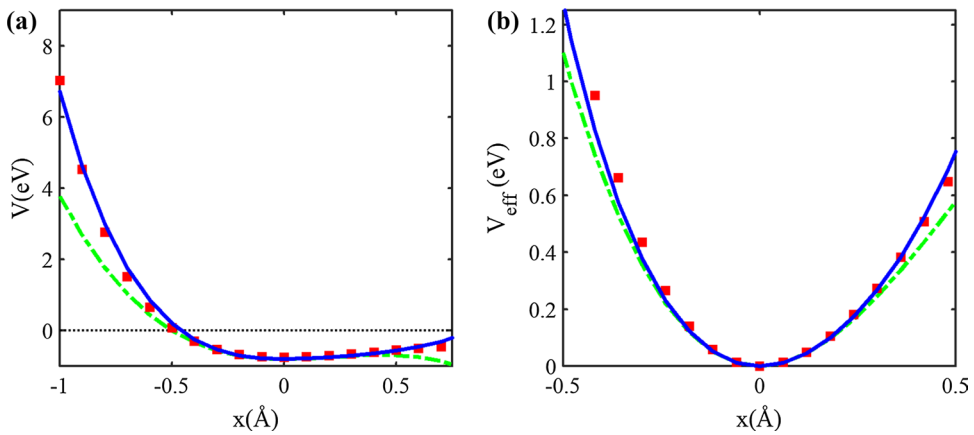

Fig. 3 Position dependence of **a** the Morse potential and **b** the AE potential of Mo obtained using the CACE model (solid blue lines), the QACE model [51] (dashed-dotted green lines), and experiment [36] (full red squares)

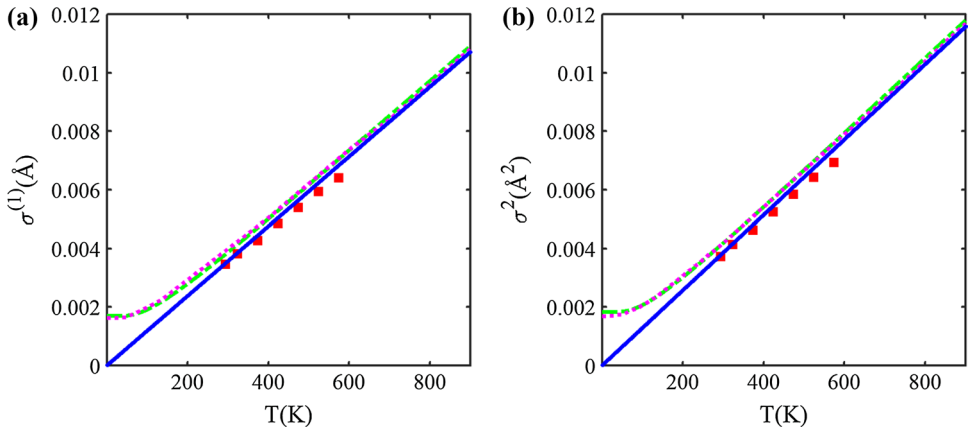

Fig. 4 Temperature dependence of the **a** first and **b** second cumulants of Mo obtained using the CACE model (solid blue lines), the QACE [51] (dashed-dotted green lines), the ACD model [42] (dotted magenta lines), and experiment [36] (full red diamonds)

are derived from the experimental values of parallel MSRD and using Eq. (27) (this procedure is the same as in Refs. [42, 51]). At 293 K, the obtained results using the CACE, QACE, and ACD models are $\sigma^{(1)} \simeq 3.5 \times 10^{-3}$ Å and $\sigma^2 \simeq 3.8 \times 10^{-3}$ Å^2, $\sigma^{(1)} \simeq 3.8 \times 10^{-3}$ Å and $\sigma^2 \simeq 4.1 \times 10^{-3}$ Å^2 [51], and $\sigma^{(1)} \simeq 3.9 \times 10^{-3}$ Å and $\sigma^2 \simeq 4.1 \times 10^{-3}$ Å^2 [42], respectively, while the experimental values are $\sigma^{(1)} \approx 3.5 \times 10^{-3}$ Å and $\sigma^2 \approx 3.7 \times 10^{-3}$ Å^2 [36].

Figure 5 shows the temperature dependence of the (a) third cumulant $\sigma^{(3)}(T)$ and (b) fourth cumulant $\sigma^{(4)}(T)$ of Mo calculated by Eqs. (29) and (30), respectively. Our calculated results using the CACE model indicate good agreement with those obtained using the QACE model [51] (only for the third cumulant), the ACD model [42], and experiment [36] as seen in Fig. 5, especially at temperatures not too low. The applicable limits of the CACE model for the third and fourth cumulants in the low-temperature region have been discussed in detail in Ref. [39]. At 293 K, the obtained results using the CACE, QACE, and ACD models are $\sigma^{(3)} \simeq 2.6 \times 10^{-5}$ Å^3 and $\sigma^{(4)} \simeq 2.3 \times 10^{-7}$ Å^4, $\sigma^{(3)} \simeq 2.7 \times 10^{-5}$ Å^3 [51], and $\sigma^{(3)} \simeq 2.4 \times 10^{-5}$ Å^3 and $\sigma^{(4)} \simeq 2.7 \times 10^{-7}$ Å^4 [42], respectively, while the experimental values are $\sigma^{(3)} \approx 2.5 \times 10^{-5}$ Å^3 and $\sigma^{(4)} \approx 2.2 \times 10^{-7}$ Å^4 [36]. If replacing the local force constants in the expressions of the EXAFS cumulants obtained from Refs. [42, 51] by the corresponding constants that are expressed in terms of the Morse potential parameters from Eq. (16). Our obtained results for the first three cumulants are the same as the corresponding results calculated from the QACE [51] and ACD [42] models in the high-temperature limit. And our obtained result for the fourth cumulant is slightly smaller than the result calculated from the ACD model.

Additionally, the ACD model describes the lattice vibrations of atoms by the phonons that have the frequencies varying from 0 to the correlated Debye frequency ω_D and depending on the wavenumber, and propagate with the speed of sound [33, 45], so the ACD model can easily treat the acoustic phonons. In contrast, the ACE model (including the QACE and CACE models) describes these vibrations by phonons that have the same correlated Einstein frequency ω_E and do not depend on the wavenumber and can interact with the electromagnetic waves [12, 51], so the ACE model can easily treat the optical phonons. The origin of this discrepancy is the presence in lattice crystals of the acoustic phonon branches that cannot be mimicked by a unique correlated Einstein frequency ω_E [57, 58]. Consequently, the ACD model can work better than the ACE model for the monatomic cubic crystals that have multiple acoustic phonons and less complex phonon density of states (PDOS), such as BCC and FCC crystals, neither is usually adequate for heterogeneous systems. Conversely, the ACE model can be very useful for the ionic crystals that have multiple optical phonons and complex PDOS, such as oxides and salts [59, 60]. As can be seen from the obtained results in Figs. 4 and 5 for Mo, The ACD, QACE, and CACE models all work effectively, in which the ACD model seems to be the best, the QACE model only calculates for the first three cumulants, and the CACE model only works well in the high-temperature region. However, the difference between these models is insignificant for high-order cumulants and in the high-temperature region because the values of high-order cumulants are quite small, and the influence of quantum effects is insignificant at high temperatures.

Thus, the temperature dependence of the first four EXAFS cumulants calculated using the present CACE model, which has satisfied all of their fundamental properties in comparison with other theoretical models and experiments at temperatures above the correlated Einstein temperature. This result shows the influence of anharmonic effects on the classical limit via thermal vibration contributions at high temperatures. It is because the anharmonicity in the EXAFS spectra appears from about room temperature.

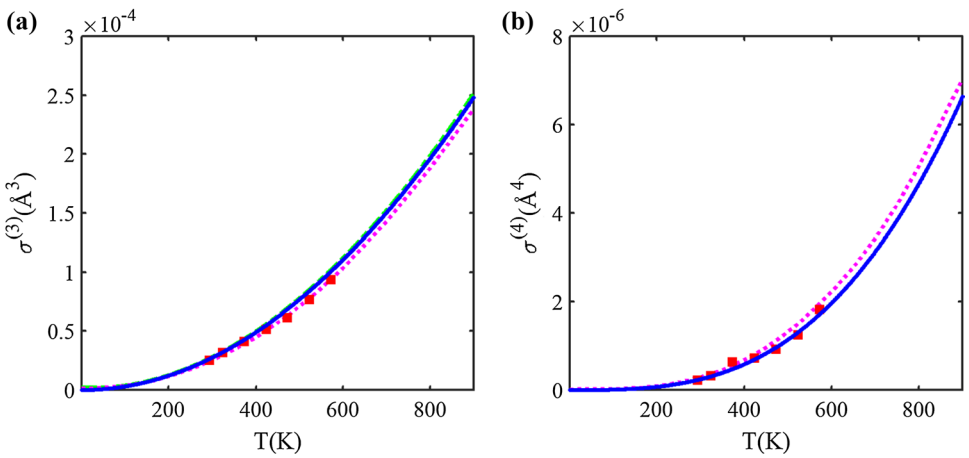

Fig. 5 Temperature dependence of the **a** third and **b** fourth cumulants of Mo obtained using the CACE model (solid blue lines), the QACE [51] (dashed-dotted green line), the ACD model [42] (dotted magenta lines), and experiment [36] (full red squares)

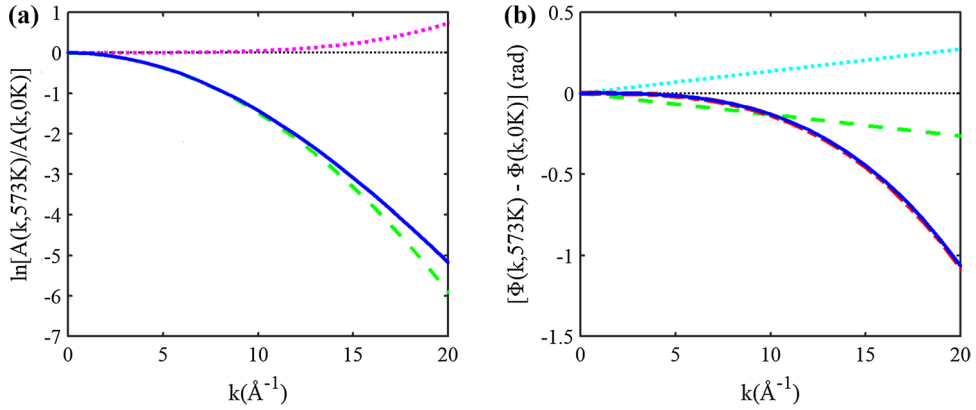

Fig. 6 Wavenumber dependence of **a** the logarithm of amplitude ratio and (b) the phase difference between temperatures 573 and 0 K of Mo obtained using the CACE model in the cases: calculating all of the terms in Eqs. (35) or (36) (solid blue lines) and calculating only one term that contains the first cumulant in Eq. (36) (dotted cyan line), the second cumulant in Eqs. (35) or (36) (dashed green lines), the third cumulant in Eq. (36) (dashed-dotted red line), and the fourth cumulant in Eq. (35) (dotted magenta line)

Figure 6 shows the wavenumber dependence of (a) the logarithm of amplitude ratio $M(k) = \ln\left[A(k, 293\,K)/A(k, 0\,K)\right]$ and (b) the phase difference $\Delta\Phi(k) = \Phi(k, 293\,K) - \Phi(k, 0\,K)$ of Mo calculated by Eqs. (35) and (36), respectively. The logarithm of amplitude ratio $M(k)$, including the contributions of terms that contain the second cumulant (henceforth denoted as $M_1(k)$) and fourth cumulant (henceforth denoted as $M_2(k)$), as seen via Eq. (35). As can be seen from Fig. 6a, our calculated result demonstrates that the contribution of $M_1(k)$ to the value of $M(k)$ is mainly. Still, the contribution of the $M_2(k)$ is also significant and reduces the value of $M(k)$, especially at large wavenumbers (high energy photoelectrons). Our obtained result of the ratio $M_2(k)/M(k)$ is about -3.2% at $k = 10$ Å^{-1} and about -14.1% at $k = 20$ Å^{-1}. The phase difference $\Delta\Phi(k)$, including the contributions of terms that contain the first cumulant (henceforth denoted as $\Delta\Phi_1(k)$), the second cumulant (henceforth denoted as $\Delta\Phi_2(k)$), and the third cumulant (henceforth denoted as $\Delta\Phi_3(k)$) as seen via Eq. (36). As can be seen from Fig. 6b, our calculated result demonstrates that the contributions of $\Delta\Phi_1(k)$ and $\Delta\Phi_2(k)$ to the value of $\Delta\Phi(k)$ are significant. Still, the contribution of $\Delta\Phi_1(k)$ is opposite and only slightly larger than the contribution of $\Delta\Phi_2(k)$, which makes them eliminate each other and influence of $\Delta\Phi_3(k)$ on the value of $\Delta\Phi(k)$ is greatest, especially at large wavenumbers. Our obtained result of the ratio $\Delta\Phi_3(k)/\Delta\Phi(k)$ is about 103.5% at $k = 10$ Å^{-1} and about 100.9 % at $k = 20$ Å^{-1}.

Consequently, the contribution of $M_2(k)$ cannot be ignored in the calculation of the logarithm of amplitude ratio $M(k)$ in Eq. (35). And the approximation $\Delta\Phi(k) \approx \Delta\Phi_3(k)$ can be satisfactory with negligible errors in the calculation of the phase difference $\Delta\Phi(k)$ in Eq. (36). It means that the influence of the fourth cumulant needs to be taken into account, while the influence of the first and second cumulants can be ignored in analyzing the anharmonic EXAFS spectra, especially at large wavenumbers.

Conclusions

The advantage of the present CACE model in comparison with other theoretical procedures is that the first four EXAFS cumulants are expressed in simple forms of temperature or parallel MSRD. These results are useful not only for predicting results of other theoretical procedures but also for reducing measurements of the experimental EXAFS data.

The contributions of the EXAFS cumulants to the anharmonic EXAFS oscillation are analyzed in detail. It discovers that the third cumulant plays an important role and has the greatest influence on the phase shift, and the fourth cumulant plays an indispensable role and significantly influences the amplitude reduction, especially at large wavenumbers. These evaluations are very useful for analyzing the anharmonic EXAFS spectra.

The present CACE model can be applied to analyze the anharmonic EXAFS spectra starting from about the correlated Einstein temperature to just before the melting point. The good agreement of our numerical results for Mo with those obtained using the QACE model, ACD model, and experiment at various temperatures, which shows the effectiveness of the present CACE model for calculating and analyzing the anharmonic EXAFS spectra. This calculation model not only applies well to BCC crystals but also can be extended to other crystal structures.

Acknowledgements This work was supported by the Institute of Research and Development, Duy Tan University, Da Nang 550000, Vietnam.

References

1. Lytle, F.W., Sayers, D.E., Stern, E.A.: Extended X-ray-absorption fine-structure technique. II. Experimental practice and selected results. Phys. Rev. B **11**, 4825–4835 (1975)
2. Beni, G., Platzman, P.M.: Temperature and polarization dependence of extended X-ray absorption fine-structure spectra. Phys. Rev. B **14**, 1514–1518 (1976)
3. Eisenberger, P., Brown, G.S.: The study of disordered systems by EXAFS: limitations. Solid State Commun. **29**, 481–484 (1979)
4. Greegor, R.B., Lytle, F.W.: Extended X-ray absorption fine structure determination of thermal disorder in Cu: comparison of theory and experiment. Phys. Rev. B **20**, 4902–4907 (1979)
5. Stern, E.A., Bunker, B.A., Heald, S.M.: Many-body effects on extended X-ray absorption fine structure amplitudes. Phys. Rev. B **21**, 5521–5539 (1980)
6. Lee, P.A., Citrin, P.H., Eisenberger, P., Kincaid, B.M.: Extended X-ray absorption fine structures-its strengths and limitations as a structural tool. Rev. Mod. Phys. **53**, 769–806 (1981)
7. Bunker, G.: Applications of the ratio method of EXAFS analysis to disordered systems. Nucl. Instrum. Methods **207**, 437–444 (1983)
8. Tröger, L., Yokoyama, T., Arvanitis, D., Lederer, T., Tischer, M., Baberschke, K.: Determination of bond lengths, atomic mean-square relative displacements, and local thermal expansion by means of soft-X-ray photoabsorption. Phys. Rev. B **49**, 888–903 (1994)
9. Dalba, G., Fornasini, P., Grazioli, M.: Local disorder in crystalline and amorphous germanium. Phys. Rev. B **76**, 11034–11043 (1995)
10. Kubo, R.: Generalized cumulant expansion method. J. Phys. Soc. Jpn. **17**, 1100–1120 (1962)
11. Rehr, J.J., Albers, R.C.: Theoretical approaches to X-ray absorption fine structure. Rev. Mod. Phys. **72**, 621–654 (2000)
12. Hung, N.V., Rehr, J.J.: Anharmonic correlated Einstein-model Debye–Waller factors. Phys. Rev. B **56**, 43–46 (1997)
13. Tranquada, J.M., Ingalls, R.: Extended X-ray-absorption fine-structure study of anharmonicity in CuBr. Phys. Rev. B **28**, 3520–3528 (1983)
14. Crozier, E.D., Rehr, J.J., Ingalls, R.: Amorphous and liquid systems. In: Koningsberger, D.C., Prins, R. (eds.) X-ray Absorption: Principles, Applications, Techniques of EXAFS, SEXAFS and XANES. Wiley, New York (1988)
15. Yokoyama, T., Ohta, T., Sato, H.: Thermal expansion and anharmonicity of solid Kr studied by extended X-ray-absorption fine structure. Phys. Rev. B **55**, 11320–11329 (1997)
16. Tien, T.S.: Advances in studies of the temperature dependence of the EXAFS amplitude and phase of FCC crystals. J. Phys. D Appl. Phys. **53**, 315303 (2020)
17. Frenkel, A.I., Rehr, J.J.: Thermal expansion and x-ray-absorption fine-structure cumulants. Phys. Rev. B **48**, 585–588 (1993)
18. Vaccari, M., Grisenti, R., Fornasini, P., Rocca, F., Sanson, A.: Negative thermal expansion in CuCl: an extended X-ray absorption fine structure study. Phys. Rev. B **75**, 184307 (2007)
19. Ahmed, S.I., Dalba, G., Fornasini, P., Vaccari, M., Rocca, F., Sanson, A., Li, J., Sleight, A.W.: Negative thermal expansion in crystals with the delafossite structure: an extended x-ray absorption fine structure study of $CuScO_2$ and $CuLaO_2$. Phys. Rev. B **79**, 104302 (2009)
20. Dalba, G., Fornasini, P.: EXAFS Debye-Waller Factor and Thermal Vibrations of Crystals. J. Synchrotron Radiat. **4**, 243–255 (1997)
21. Dalba, G., Fornasini, P., Grisenti, R., Pasqualini, D., Diop, D., Monti, F.: Anharmonicity effects on the extended x-ray-absorption fine structure: the case of cadmium selenide. Phys. Rev. B **58**, 4793–4802 (1998)
22. Sevillano, E., Meuth, H., Rehr, J.J.: Extended X-ray absorption fine structure Debye–Wailer factors. I. Monatomic crystals. Phys. Rev. B **20**, 4908–4911 (1979)
23. Fujikawa, T., Miyanaga, T.: Quantum statistical approach to Debye–Waller factors in EXAFS, EELS, and ARXPS. I. Anharmonic contribution in plane-wave approximation. J. Phys. Soc. Jpn. **62**, 4108–4122 (1993)
24. Miyanaga, T., Fujikawa, T.: Quantum statistical approach to Debye–Waller factor in EXAFS, EELS, and ARXPS. III. Applicability of Debye and Einstein approximation. J. Phys. Soc. Jpn. **63**, 3683–3690 (1994)
25. Miyanaga, T., Fujikawa, T.: Quantum statistical approach to Debye–Waller factor in EXAFS, EELS and ARXPS. II. Application to one-dimensional models. J. Phys. Soc. Jpn. **63**, 1036–1052 (1994)
26. Yokoyama, T.: Path-integral effective-potential method applied to extended X-ray-absorption fine-structure cumulants. Phys. Rev. B **57**, 3423 (1998)
27. Yokoyama, T.: Path-integral effective-potential theory for EXAFS cumulants compared with the second-order perturbation. J. Synchrotron Radiat. **6**, 323–325 (1999)
28. Poiarkova, A.V., Rehr, J.J.: Multiple-scattering X-ray-absorption fine-structure Debye–Waller factor calculations. Phys. Rev. B **59**, 948–957 (1999)
29. Beccara, S.A., Dalba, G., Fornasini, P., Grisenti, R., Pederiva, F., Sanson, A., Diop, D., Rocca, F.: Local thermal expansion in copper: extended X-ray-absorption fine-structure measurements and path-integral Monte Carlo calculations. Phys. Rev. B **68**, 140301 (2003)
30. Beccara, S.A., Fornasini, P.: Path-integral Monte Carlo calculation of the effects of thermal disorder in extended X-ray-absorption fine structure of copper. Phys. Rev. B **77**, 172304 (2008)
31. Vila, F.D., Rehr, J.J., Rossner, H.H., Krappe, H.J.: Theoretical X-ray absorption Debye–Waller factors. Phys. Rev. B **76**, 014301 (2007)
32. Vila, F.D., Lindahl, V.E., Rehr, J.J.: X-ray absorption Debye–Waller factors from ab initio molecular dynamics. Phys. Rev. B **85**, 024303 (2012)
33. Hung, N.V., Trung, N.B., Kirchner, B.: Anharmonic correlated Debye model Debye–Waller factors. Phys. B **405**, 2519–2525 (2010)
34. Stern, E.A., Livins, P., Zhang, Z.: Thermal vibration and melting from a local perspective. Phys. Rev. B **43**, 8850–8860 (1991)
35. Pirog, I.V., Nedoseikina, T.I., Zarubin, I.A., Shuvaev, A.T.: Anharmonic pair potential study in face-centered-cubic structure metals. J. Phys.: Condens. Matter **14**, 1825–1832 (2002)
36. Pirog, I.V., Nedoseikina, T.I.: Study of effective pair potentials in cubic metals. Phys. B **334**, 123–129 (2003)
37. Vlasenko, V.G., Podsukhina, S.S., Kozinkin, A.V., Zubavichus, YaV: Determination of the melting temperature of palladium nanoparticles by X-ray absorption spectroscopy. Phys. Solid State **58**, 421–426 (2016)
38. Hung, N.V., Tien, T.S., Duc, N.B., Vuong, D.Q.: High-order expanded XAFS Debye–Waller factors of HCP crystals based on classical anharmonic correlated Einstein model. Mod. Phys. Lett. B **28**, 1450174 (2014)
39. Tien, T.S., Hung, N.V., Tuan, N.T., Nam, N.V., An, N.Q., Thuy, N.T.M., Lien, V.T.K., Nghia, N.V.: High-order EXAFS cumulants

of diamond crystals based on a classical anharmonic correlated Einstein model. J. Phys. Chem. Solids **134**, 307–312 (2019)
40. Rehr, J.J., Zabinsky, S.I., Ankudinov, A., Albers, R.C.: Atomic-XAFS, and XANES. Phys. B **208–209**, 23–26 (1995)
41. Mahan, G.D.: Many-Particle Physics, 2nd edn. Plenum, New York (1990)
42. Hung, N.V., Hue, T.T., Khoa, H.D., Vuong, D.Q.: Anharmonic correlated Debye model high-order expanded interatomic effective potential and Debye–Waller factors of bcc crystals. Phys. B **503**, 174–178 (2016)
43. Duc, N.B., Tho, V.Q., Hung, N.V., Khoa, D.Q., Hieu, H.K.: Anharmonic effects of gold in extended X-ray absorption fine structure. Vacuum **145**, 272–277 (2017)
44. Duc, N.B., Tho, V.Q., Tien, T.S., Khoa, D.Q., Hieu, H.K.: Pressure and temperature dependence of EXAFS Debye–Waller factor of platinum. Radiat. Phys. Chem. **149**, 61–64 (2018)
45. Duc, N.B., Hung, N.V., Khoa, H.D., Vuong, D.Q., Tien, T.S.: Thermodynamic properties and anharmonic effects in XAFS based on anharmonic correlated debye model Debye–Waller factors. Adv. Mater. Sci. Eng. **2018**, 3263170 (2018)
46. Hung, N.V., Thang, C.S., Duc, N.B., Vuong, D.Q., Tien, T.S.: Temperature dependence of theoretical and experimental Debye–Waller factors, thermal expansion and XAFS of metallic zinc. Phys. B **521**, 198–203 (2017)
47. Hung, N.V., Thang, C.S., Duc, N.B., Vuong, D.Q., Tien, T.S.: Advances in theoretical and experimental XAFS studies of thermodynamic properties, anharmonic effects and structural determination of fcc crystals. Eur. Phys. J. B **90**, 256 (2017)
48. Hung, N.V., Duc, N.B., Vuong, D.Q., Toan, N.C., Tien, T.S.: Advances in EXAFS studies of thermodynamic properties and anharmonic effects based on Debye–Waller factors. Applications to semiconductors. Vacuum **169**, 108872 (2019)
49. Fornasini, P., Grisenti, R., Dapiaggi, M., Agostini, G., Miyanaga, T.: Nearest-neighbour distribution of distances in crystals from extended X-ray absorption fine structure. J. Chem. Phys. **147**, 044503 (2017)
50. Duc, N.B., Tho, N.Q.: Dependence of cumulants and thermodynamic parameters on temperature and doping ratio in extended X-ray absorption fine structure spectra of cubic crystals. Phys. B **552**, 1–5 (2019)
51. Vuong, D.Q., Hung, N.V.: Impurity effects in Debye–Waller factors of bcc crystals based on anharmonic correlated Einstein model. J. Mod. Phys. Lett. B **33**, 1950078 (2019)
52. Freund, J., Ingalls, R., Crozier, E.D.: Extended X-ray-absorption fine-structure study of copper under high pressure. Phys. Rev. **39**, 12537–12547 (1989)
53. Yokoyama, T., Kobayashi, K., Ohta, T., Ugawa, A.: Anharmonic interatomic potentials of diatomic and linear triatomic molecules studied by extended X-ray-absorption fine structure. Phys. Rev. B **53**, 6111–6122 (1996)
54. Morse, P.M.: Diatomic molecules according to the wave mechanics. II. Vibrational levels. Phys. Rev. **34**, 57–64 (1929)
55. Girifalco, L.A., Weizer, V.G.: Application of the Morse potential function to cubic metals. Phys. Rev. **114**, 687–690 (1959)
56. Comaschi, T., Balerna, A., Mobilio, S.: Thermal dependent anharmonicity effects on gold bulk studied by extended X-ray-absorption fine structure. J. Phys. Condens. Matter **21**, 325404 (2009)
57. Grimvall, G.: Thermophysical Properties of Materials, 1st edn. North-Holland, Amsterdam (1999). **Kindle Edition**
58. Grosso, G., Parravicini, G.P.: Solid State Physics, 1st edn. Academic Press, London (2000)
59. Kittel, C.: Introduction to Solid State Physics, 6th edn. Wiley, New York (1986)
60. Ashcroft, N.L., Mermin, N.D.: Solid State Physics. Holt. Rinehart & Winston, New York (1976)